IOP Publishing Journal of Physics D: Applied Physics
J. Phys. D: Appl. Phys. **40** (2007) 3094–3101 doi:10.1088/0022-3727/40/10/013

Onset voltage of negative corona on stranded conductors

M M El-Bahy, M Abouelsaad, N Abdel-Gawad and M Badawi

Faculty of Engineering, Benha University, Cairo, Egypt

Received 3 February 2007, in final form 9 March 2007
Published 4 May 2007
Online at stacks.iop.org/JPhysD/40/3094

Abstract
Theoretical investigation of the onset voltage of negative corona on stranded conductors is described in this paper. The method of calculation is based on the criterion developed for the formation of repetitive negative corona Trichel pulses. This calls first for an accurate calculation of the electric field in the vicinity of stranded conductors. The investigated gap is a three-dimensional field problem. To solve this problem, a new modification of the charge simulation technique is presented, where the simulation charges are helical of infinite length. Laboratory measurements of the onset voltage on stranded conductors are carried out to check the accuracy of the present calculations. The effects of varying the field nonuniformity on the onset voltage values are investigated. The calculated onset voltage values for stranded conductors agree satisfactorily with those measured experimentally.

1. Introduction

Corona can limit the performance of any given configuration of electrical conductors [1]. Hence, the onset voltage of the corona is an important design consideration for any set of stressed conductors. Knowledge of this voltage is of paramount importance in gas insulated systems. The problems associated with the corona discharge on high voltage (HV) transmission line conductors are power loss, audible noise and electromagnetic interference [2]. These problems can limit the voltage to which the line can be energized.

Gas insulated substations (GIS) are successfully used for HV alternating current (ac) power systems. With a tremendous increase in the power transmitted, direct current (dc) transmission has become competitive and many dc transmission lines are installed everywhere in the world [3]. This has created a growing interest in the study of a self-maintained corona discharge on dc transmission lines. Onset corona fields on smooth cylindrical conductors for both polarities are believed to be approximately equal and in agreement with experiment, within the limits of experimental error [4]. Hence, in this paper onset voltage of corona may be predicted by calculating the onset voltage of negative polarity.

The corona onset voltage for a smooth cylindrical conductor in atmospheric air is well described by simple empirical formulae based on experimental data [6]. These formulae are of great utility because the onset corona field E_o can be calculated for any radius without involved numerical calculations. However, at normal pressure and temperature, these formulae predict values of E_o that vary widely for the same gap geometry and are given for both polarities by Lowke and Alessandro as [4]

$$E_o(\mathrm{kV\,cm^{-1}}) = 25\left(1 + \frac{0.4}{\sqrt{R}}\right), \tag{1}$$

against the empirical formula presented before for calculating the onset field of negative corona [5],

$$E_o(\mathrm{kV\,cm^{-1}}) = A + \frac{B}{\sqrt{R}}, \tag{2}$$

where R is the conductor radius in cm and A and B lie in the ranges 29.4–40.3 and 7.34–9.92, respectively [5]. Peek and co-workers [6] reported A and B to be equal to 31 and 9.55.

Practical transmission lines are normally of stranded construction and often contain surface irregularities. Stranded conductors are composed of a number of small wires arranged in layers around each other. The first layer around the centre strand is made up of 6 strands, the second layer is made up of 12 additional strands and the third layer is made up of 18 additional strands, etc. Thus, stranded conductors are composed of 7, 19, 37, ... strands in continuing fixed increments and the external layer twists around interior layers in a helical (spiral) form.

Conductors are stranded mainly to increase their flexibility. Stranding distorts the field in the immediate vicinity of the conductor and reduces the corona onset voltage. A semi-analytic expression was used to calculate the electric field in a coaxial arrangement of infinitely long

energized stranded conductors placed inside the centre of a grounded cylinder [1]. The ratio of the maximum surface electric field of the stranded conductor to that of smooth cylindrical conductors was conducted using image theory [7] and conformal mapping [8]. The influence of stranding on the corona onset voltage of a smooth cylindrical conductor was investigated experimentally many years ago by Peek and co-workers [6]. They characterized the influence of the strands by introducing a surface irregularity factor, m, defined as the ratio of the corona onset voltage of a stranded conductor to that of a smooth cylindrical conductor with the same outer diameter. The value of m equals unity for a perfectly smooth conductor and is less than 1 for stranded conductors. Peek and co-workers gave m the range 0.72–0.82 for 7-stranded conductors. In Whitehead's investigation [9], the number of strands in the outer layer, n_o, was varied from 3 to 9. Their data for m ranged from 0.85 to 0.92 and illustrated the physically intuitive result that conductors with a large number of strands behaved more like smooth conductors than conductors with a small number of strands. Hence, there are no definite values of m and the onset voltage. In addition, the onset voltage depends not only on the value of the surface field but also on the field distribution in the vicinity of the conductor and the properties of the gas in which the conductor is located. Therefore, the empirical formulae predict inaccurate values of the onset voltage of corona. This motivates the authors to conduct the present study.

The main target of this paper is to investigate the effect of stranding on the onset voltage of negative corona on stranded conductors positioned in air opposite a ground plane. The onset voltage calculation is based on the criterion developed for the formation of repetitive negative corona Trichel pulses. This criterion calls for the assessment of the electric field in the vicinity of the stressed conductor. An accurate charge simulation technique (CST) is used for field calculation in the vicinity of the stressed conductors. This approach is different from the techniques previously published in the literature [1, 7, 8]. As the external layer twists around the interior layers in a helical shape, the simulating charges take the same helical form. To the best of our knowledge, the helical charge has not yet been reported in the literature. Also, laboratory measurements of the onset voltage of corona on 7-stranded conductors are carried out. The effects of varying the field nonuniformity on the onset voltage values are investigated. The calculated onset voltage values for stranded conductors are compared with those measured experimentally and with values obtained by empirical formulae.

2. Twisting of the external layer of stranded conductors

The outer layer of stranded conductors twists around the inner layers in a helical form. The locus of a point $a(x, y, z)$ which moves in a uniform motion along a generatrix around the circular conductor is called a helix (appendix A) [10]. The length of one complete revolution of a point $a(x, y, z)$, around the conductor axis is called a pitch and it is repeated along the helix. Practically, the pitch length (L_p) equals the pitch factor (PF) times the overall diameter ($2R$) of the stranded conductor [11] and PF for 7-, 19- and 37-stranded conductors

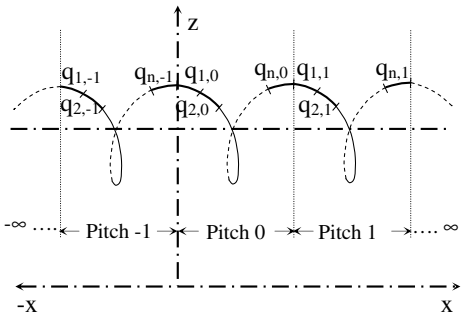

Figure 1. Division of the helical charge, q_h, into an infinite number of pitches $(-\infty, \ldots, -k, \ldots, -1, 0, 1, \ldots k, \ldots, \infty)$ and division of that charge in each pitch into n finite line charges.

equals 16–18, 14–16 and 12–14, respectively [11]. Hence, $L_p = 2R\times$ PF, where PF is chosen to be 17, 15 or 13 for 7-, 19- or 37-stranded conductors, respectively. The location of point $a(x, y, z)$ is related to L_p and the conductor radius R as obtained in appendix A by equations (A2)–(A4).

3. Method of analysis

3.1. Electric field calculation around stranded conductor

The analysis is based on CST in which the distributed charges on the surface of the stressed conductor are replaced by a set of fictitious simulation charges arranged inside the external layer of stranded conductors. To maintain the ground plane at zero potential, images of the simulation charges are considered. The satisfaction of the pertinent boundary condition results in a set of equations whose simultaneous solution determines the unknown simulation charges. Knowing the simulating charges, the electric potential and field can be calculated at any point in the investigated gap.

3.1.1. Simulation technique. The simulating charges are placed inside each strand of the external layer and take the same helical shape as the strand and repeat along the x-axis after a pitch. The stranded conductor is assumed infinitely long and segmented into an infinite number of pitches $(-\infty, \ldots, -k, \ldots, -1, 0, 1, \ldots k, \ldots, -\infty)$. The number of simulating helical charges, q_h, is assumed to be 3 times the number of strands in the outer layer ($3 \times n_o$). In each pitch, any helical charge is divided into n finite line charges, having length ℓ and equal projections along the x-axis, figure 1. Hence, the number of simulating finite line charges in each pitch equals N ($N = 3 \times n \times n_o$); however, the only unknown simulating charges are those in pitch-0 because the pitches are repeated. Each finite line charge inclusive of its image will be assigned to a Cartesian coordinate system (x_1, y_1, z_1) and (x_2, y_2, z_2), respectively [12]. By the transformation of the coordinates, an arbitrary point $A_i(x, y, z)$ is referred to these new coordinates. A coordinate transformation will be conducted for the complete arrangement of simulation line charges.

Coordinates of simulating finite line charges. Figure 2 shows a cross section of a 7-stranded conductor which has $n_o = 6$, an overall radius R and a gap height H. Inside each strand of the outer layer, the three simulation helical charges q_{h1}, q_{h2} and

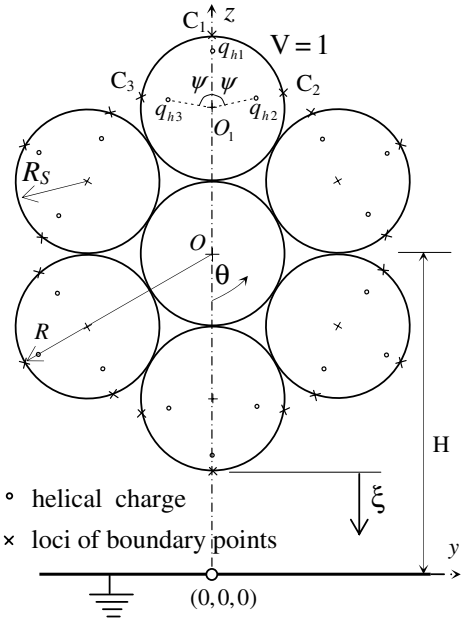

Figure 2. The location of helical charges and contour points loci in the cross section of a 7-stranded conductor.

q_{h3} in the y–z plane are assumed to be spaced radially from the strand centre at distances $f_1 R_s$, $f_2 R_s$ and $f_3 R_s$, where R_s is the strand radius, f_1, f_2 and f_3 are fractions greater than 0 and less than 1. The angle ψ defines the relative angular positions of q_{h2} and q_{h3}.

Coordinates of boundary points. To satisfy the boundary conditions, a boundary point is chosen on the strand surface corresponding to each finite line charge. Hence, N boundary points are chosen for pitch-0 on the stranded conductor surface. Each boundary point lies on its locus at the middle of the corresponding simulation line charge, figure 2.

3.1.2. Potential calculation. The potential ϕ_i at an arbitrary contour point $A_i(x, y, z)$, due to the simulation line charges Q_j ($Q_j = q_{j,0}$, $j = 1, 2, \ldots, N$), is calculated by the relation

$$\phi_i = \sum_{j=1}^{j=N} P_{i,j} Q_j, \tag{3}$$

where $P_{i,j}$ is the summation of potential coefficients $p_{i,j,k}$ at the point $A_i(x, y, z)$ due to all simulation line charges

$$P_{i,j} = \sum_{k=-\infty}^{k=\infty} p_{i,j,k}, \tag{4}$$

where the potential coefficient $p_{i,j,k}$ is expressed as [13]

$$p_{i,j,k} = \frac{1}{4\pi\varepsilon\ell_j} \ln\left(\frac{\left[(\ell_j - x_{1j}) + \gamma_{1j}\right]}{\left[(-x_{1j}) + \delta_{1j}\right]} \frac{\left[(-x_{2j}) + \gamma_{2j}\right]}{\left[(\ell_j - x_{2j}) + \delta_{2j}\right]}\right) \tag{5}$$

where

$$\gamma_{1j} = \sqrt{(\ell_j - x_{1j})^2 + y_{1j}^2 + z_{1j}^2}, \qquad \gamma_{2j} = \sqrt{x_{2j}^2 + y_{2j}^2 + z_{2j}^2},$$

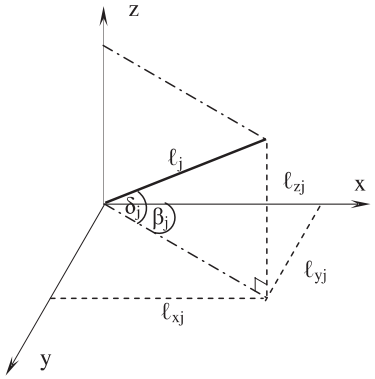

Figure 3. The inclination angles δ_j and β_j of line charge having length ℓ_j on the x–y and the x–z planes, respectively.

$$\delta_{1j} = \sqrt{x_{1j}^2 + y_{1j}^2 + z_{1j}^2}, \qquad \delta_{2j} = \sqrt{(\ell_j - x_{2j})^2 + y_{2j}^2 + z_{2j}^2}.$$

Equating the applied voltage with the calculated potential at the selected boundary points results in a set of equations whose solutions determine the unknown simulation charges.

3.1.3. Electric field calculation. It is well known that the electric field intensity E is the negative gradient of the potential. The differentiation of potential ϕ_i in the coordinate systems (x_1, y_1, z_1) and (x_2, y_2, z_2) is conducted separately. Thus, the components of the electric field, ($E_{x1i,j}$, $E_{y1i,j}$, $E_{z1i,j}$, $E_{x2i,j}$, $E_{y2i,j}$ and $E_{z2i,j}$), of charge Q_j and its image in the coordinate systems (x_1, y_1, z_1) and (x_2, y_2, z_2) are obtained, respectively. These components must be transformed back and added into the main coordinate system (x, y, z). Hence, for each finite line charge Q_j and its image, at a contour point $A_i(x, y, z)$, the field intensity components $E_{xi,j}$, $E_{yi,j}$ and $E_{zi,j}$ are

$$\begin{aligned} E_{xi,j} &= (E_{x1i,j} + E_{x2i,j}) \cos\,\delta_j \cos\,\beta_j \\ &\quad -(E_{y1i,j} + E_{y2i,j}) \sin\,\beta_j \\ &\quad -(E_{z1i,j} - E_{z2i,j}) \sin\,\delta_j \cos\beta_j, \\ E_{yi,j} &= (E_{x1i,j} + E_{x2i,j}) \cos\,\delta_j \sin\beta_j \\ &\quad +(E_{y1i,j} + E_{y2i,j}) \cos\,\beta_j \\ &\quad -(E_{z1i,j} - E_{z2i,j}) \sin\,\delta_j \sin\beta_j, \\ E_{zi,j} &= (E_{x1i,j} - E_{x2i,j}) \sin\,\delta_j \\ &\quad +(E_{z1i,j} + E_{z2i,j}) \cos\,\delta_j, \end{aligned} \tag{6}$$

where the angles δ_j and β_j are the inclination angles of a line charge having length ℓ_j on the x–y and x–z planes, respectively, as shown in figure 3.

Hence, the field intensity components E_{xi}, E_{yi} and E_{zi} at point $A_i(x, y, z)$ are obtained as follows:

$$E_{xi} = \sum_{j=1}^{j=N} E_{xi,j},$$

$$E_{yi} = \sum_{j=1}^{j=N} E_{yi,j},$$

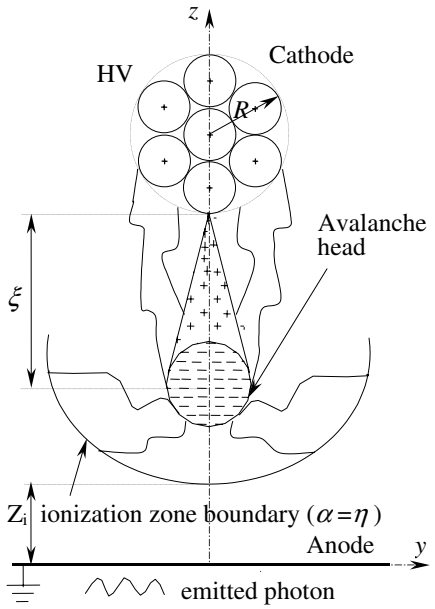

Figure 4. Development of the primary avalanche along the gap axis in the negative onset of corona.

$$E_{zi} = \sum_{j=1}^{j=N} E_{zi,j}.$$

Then the field intensity at that point is calculated by the relation

$$E_i = \sqrt{E_{xi}^2 + E_{yi}^2 + E_{zi}^2}. \tag{7}$$

4. Onset criterion of negative corona

When the electric field strength in the vicinity of the stranded conductor surface reaches the onset value for ionization of air molecules by electron collision, a primary avalanche starts to develop along the gap axis away from the conductor, figure 4, where the field assumes maximum values. With the growth of the avalanche, more electrons develop at its head, more photons are emitted in all directions and more positive ions are left in the avalanche's wake. The avalanche growth takes place under the combination of the field due to the applied voltage and the field of the positive ions in the wake of the avalanche itself. The growth of the avalanche continues as long as Townsend's first ionization coefficient, $\alpha(\xi)$, is greater than the electron attachment coefficient, $\eta(\xi)$, and terminates at $z = Z_i$, i.e. at the ionization-zone boundary, $(\alpha(\xi) = \eta(\xi))$ [14], where the electrons get attached to the air molecules and form negative ions.

For a successor avalanche to be started, the preceding avalanche should somehow provide an initiating electron at the stressed electrode surface, possibly by photoemission, positive-ion impact, metastable action or field emission. Field emission is possible only at field strengths exceeding 5×10^7 V m^{-1}. Electron emission by positive-ion impact is more than two orders of magnitude less frequent than that by photoemission. Metastables have been reported to have an effect approximately equal to that of positive-ion impact. Therefore, only the first mechanism (electron emission from the cathode by photons) was considered in the mathematical formulation of the onset criterion [15], where at least one photoelectron ($N_{\mathrm{eph}} = 1$) is emitted by the photons of the primary avalanche to keep the discharge self-sustaining [14], i.e.

$$N_{\mathrm{eph}} = \gamma_{\mathrm{ph}} \int_{H-R}^{Z_i} \alpha(\xi) g(\xi) \exp\left[\int_{H-R}^{Z_i} (\alpha(\xi) - \eta(\xi))\, \mathrm{d}\xi\right] \times \exp(-\mu\xi)\, \mathrm{d}\xi, \tag{8}$$

where γ_{ph} is Townsend's second coefficient due to the action of photons, and Z_i is the distance measured along the gap axis determining the ionization-zone boundary, figure 4, and $g(\xi)$ is a geometric factor to account for the fact that some photons are not received by the cathode (appendix B) [16]. The condition for a new (successor) avalanche to develop is

$$N_{\mathrm{eph}} \geqslant 1. \tag{9}$$

The onset voltage of corona does not appear explicitly in relation (8). However, the values of α, η which are given in [14] are affected by the applied voltage. The onset voltage is the critical value, which fulfils equality (9).

5. Experimental set-up and technique

The experiments were carried out in atmospheric air using 7-strand conductors of outer radii 1, 1.25 and 1.5 mm. The conductor height above the ground plane was varied from 0.11 to 0.56 m. This investigates the effects of varying the field nonuniformity on the onset voltage values. The length and the width of the plane electrode are 2 m and 1 m, respectively. The plane was grounded through a 30 kΩ resistor. A HV dc source (Hipotronics, Model 800PL-10MA series) was employed to energize the stranded conductor up to 80 kV and 10 mA. The overall accuracy of voltage measurement was considered to be within ± 2%. The stressed conductor is connected to the HV source through a water resistance of 1 MΩ as a current-limiting resistor. The voltage drop across the 30 kΩ resistor was fed to an oscilloscope. To determine the corona onset voltage, the applied voltage was raised to about 90% of the expected value at a rate of 1 kV s^{-1} and thereafter at a rate of 0.1 kV s^{-1} until the initiation of the corona pulses on the oscilloscope takes place [17]; the applied voltage is the corona onset value. The time interval between two successive applied voltages was a minimum 1 min. At least 10 measurements were taken to estimate the mean of each measuring point. The relative standard deviation of the mean values was generally smaller than 1.3%. The tests were conducted in laboratory air at room temperature (about 22–25 °C), atmospheric pressure and low humidity.

6. Results

To check the accuracy of the charge simulation, check points are selected over the conductor circumference which lies midway between two successive boundary points found on the same locus. The potential and the deviation angle of the field at the conductor surface are assessed at the check points to check how well the boundary condition is satisfied. This check was made for practical ranges of 7-, 19- and

37-strand conductor radii; these ranges are 1–6.5 mm, 4.5–11.4 mm and 7.5–12.5 mm, respectively [11]. The accuracy remained the same for these investigated ranges as given for samples computed at the gap height $H = 1$ m.

The accuracy of a simulation depends strongly on the assumptions concerned with the choice of the number and the coordinates of the simulation charges. In pitch-0, the number of finite line charges was assumed to be $N = 3n \times n_o$. The best value of n was found to be 40. Hence, $N = 720$, 1440 and 2160 for 7-, 19- and 37-stranded conductors, respectively. The effective number of pitches $(1+2k)$ for these stranded conductors was found to depend on the gap height, H, wherever the best value of k was found to be an integer of $(80H + 12)$, i.e. for $H = 1$ m, k is equal to 92 pitches. As a result the effective length achieving the simulation accuracy of the stranded conductor will be equal to $[1+2\times(80H+12)]\times 2R\times$ PF. It depends on the gap height, the conductor radius and the type of stranding. Also, the accuracy of a simulation was found to be highly influenced by the variables f_1, f_2 and the angle ψ. Acceptable accuracy is achieved when these factors take values of (0.23, 0.5 and 109°), (0.17, 0.17 and 60°) and (0.22, 0.22 and 75°) for 7-, 19- and 37-stranded conductors, respectively.

At the circumference of the check points, the percentage errors of the potential and the electric field deviation angle in the y–z plane are calculated. Figure 5 shows the percentage errors of the calculated potential for 7-, 19- and 37-strand conductors. Over most of the stranded conductor surfaces (except the narrow zones that lie near the contact points of the outer layer strands), the electric field deviation angle does not exceed 3°, 3.4° and 1.3° for 7-, 19- and 37-stranded conductors, respectively. Figure 6 shows the electric field distribution for 7-strand conductors around the conductor circumference and along the pitch length at the line facing the ground.

Figure 7 gives an example of the electric field distribution near the stressed conductor for smooth and stranded conductors with different values of n_o at $V = 1$ kV, $R = 10$ mm and $H = 1$ m. The calculated values of the onset voltage of corona for smooth and stranded conductors at $R = 10$ mm are shown in figure 8.

The surface irregularity factor m was calculated for various numbers of strands in the outer layer n_o at varying conductor radii, R, and gap height, H, as shown in figure 9. At the gap height $H = 1$ m, this factor decreases with an increase in the conductor radius over the range 1–20 mm, figure 9(a). The decrease in this factor is smaller in the case of $R = 10$ mm and H varies from 0.1 to 1 m. Also, it is shown that as n_o increases m approaches the value of a smooth cylindrical conductor ($m = 1$) and it has a definite value at a certain conductor radius, gap height and number of strands in the outer layer n_o.

Figure 10 shows the increase in the calculated and measured onset voltage values with increasing gap height H for 7-strand conductors having radii 1, 1.25 and 1.5 mm.

The calculated and measured onset voltages are compared with those estimated by Peek and co-workers [6] and Lowke and Alessandro [4] formulae, at the maximum value of m (= 0.82) which was assumed before by Peek [6].

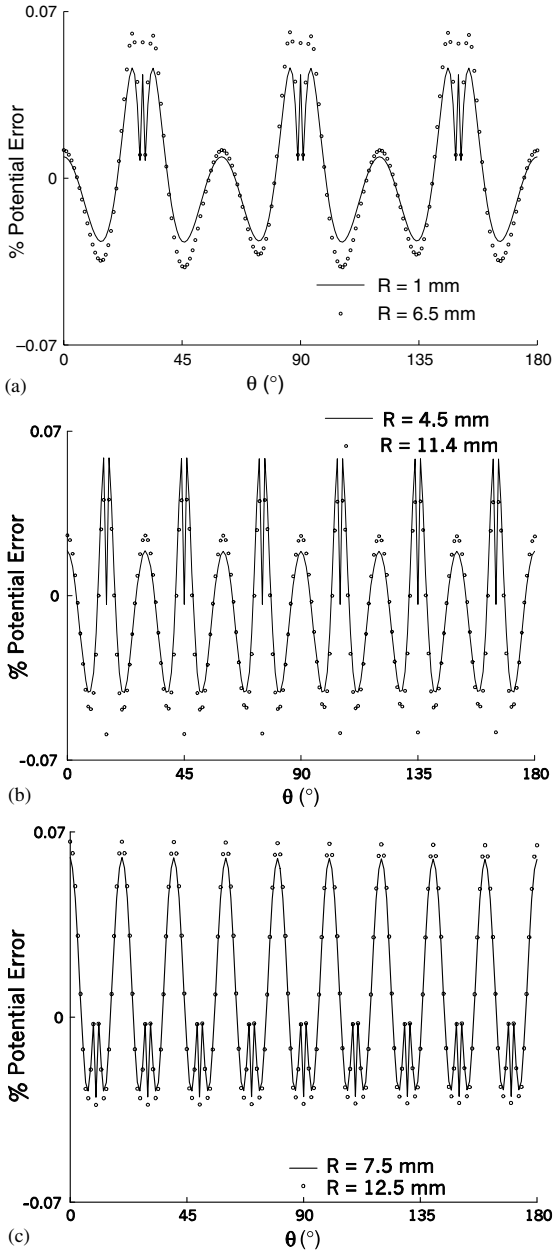

Figure 5. The variation of per cent potential errors at the check points around the circumferences of practical 7-, 19- and 39-strand conductors, respectively.

7. Discussion

In figure 5 the maximum per cent error does not exceed 0.07%. Potential errors on the electrode surface of less than 0.1% are considered reasonable for an accurate field solution [18]. The field values near the contact points of the outer layer strands are very low as shown in figure 6. Hence, the field deviation angle error near these points has no effect on the onset voltage of corona. Figure 7 gives two properties of the results. First, the peak values of the surface electric field divided by the peak value (E_{pu}) for a smooth cylindrical conductor for $n_o = 6$, 12 and 18 strands equal 1.415, 1.43 and 1.441, respectively, against the values of 1.407, 1.436 and 1.445 obtained theoretically before using conformal mapping,

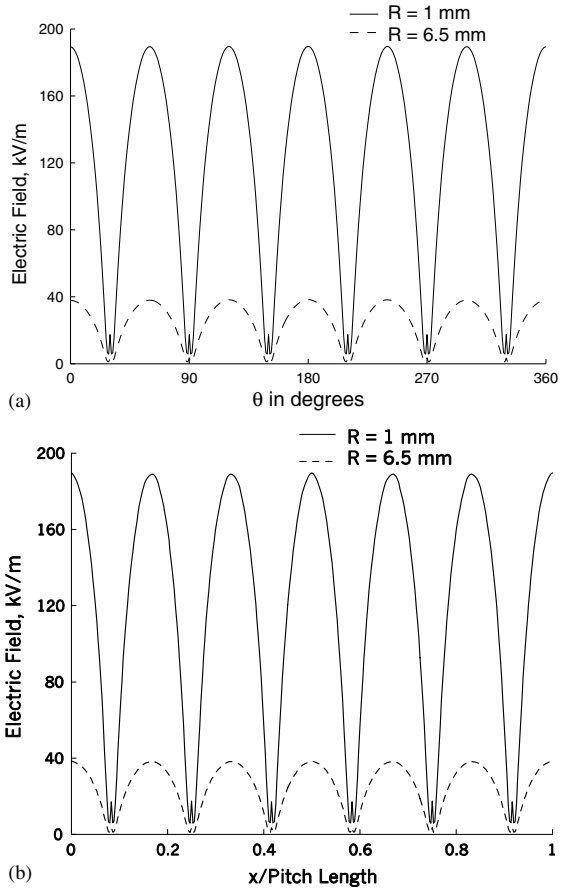

Figure 6. Electric field distribution for 7-strand conductors: (*a*) around the conductor circumference and (*b*) along the pitch length at the line facing the ground.

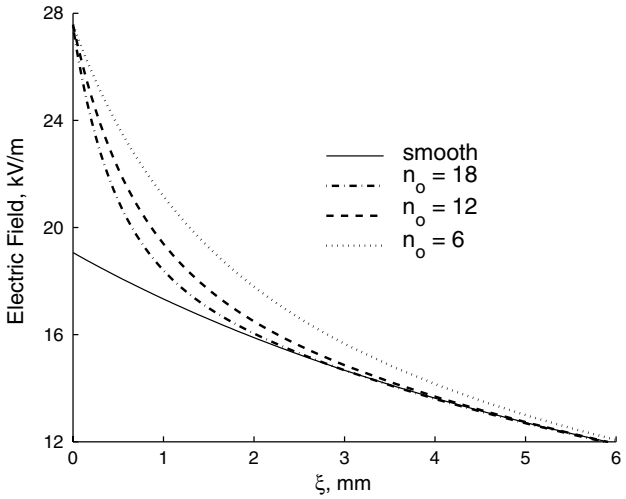

Figure 7. Electric field distribution for smooth and stranded conductors ($V = 1$ kV, $R = 10$ mm and $H = 1$ m).

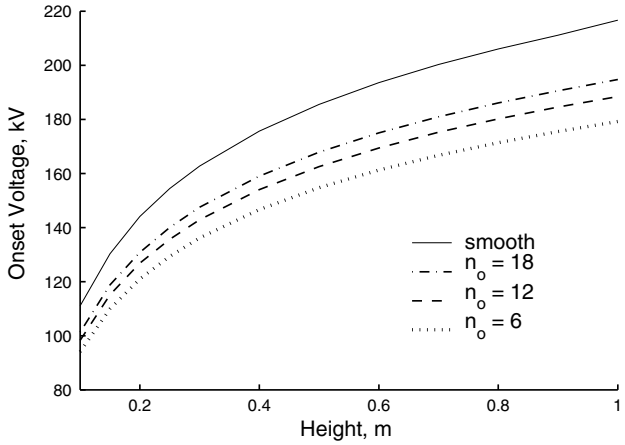

Figure 8. Calculated values of the onset voltage of corona for smooth and stranded conductors at $R = 10$ m.

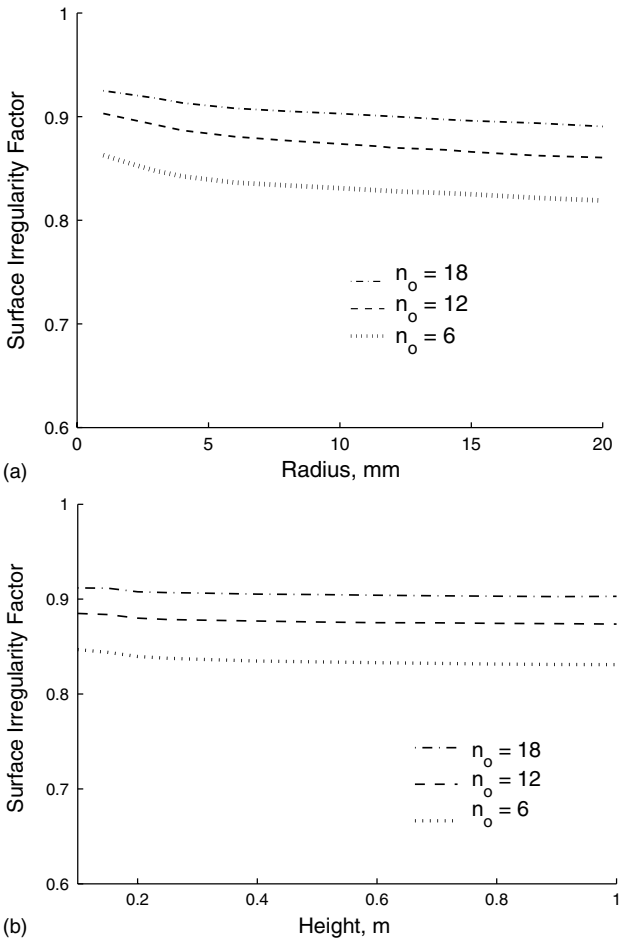

Figure 9. Predicted surface irregularity factor, m, for $n_o = 6$, 12 and 18: (*a*) the variation of m as a function of the conductor radius R at a gap height $H = 1$ m, (*b*) the variation of m as a function of the gap height H at the conductor radius $R = 10$ mm.

for the same radius and gap height [8]. These values indicate that the surface field is nearly independent of n_o and is in agreement with previous investigations [1,7] that assigned 1.4 for the value of E_{pu}, i.e. independent of n_o. Second, the larger the n_o, the smaller the region over which the electric field deviates from that of a smooth conductor; this region approaches zero as $n_o \to \infty$. This explains why the corona onset voltage for $n_o = 18$ is greater than both the onset voltage values for $n_o = 6$ and 12 and approaches that of a smooth cylindrical conductor, figure 8. The industrial context

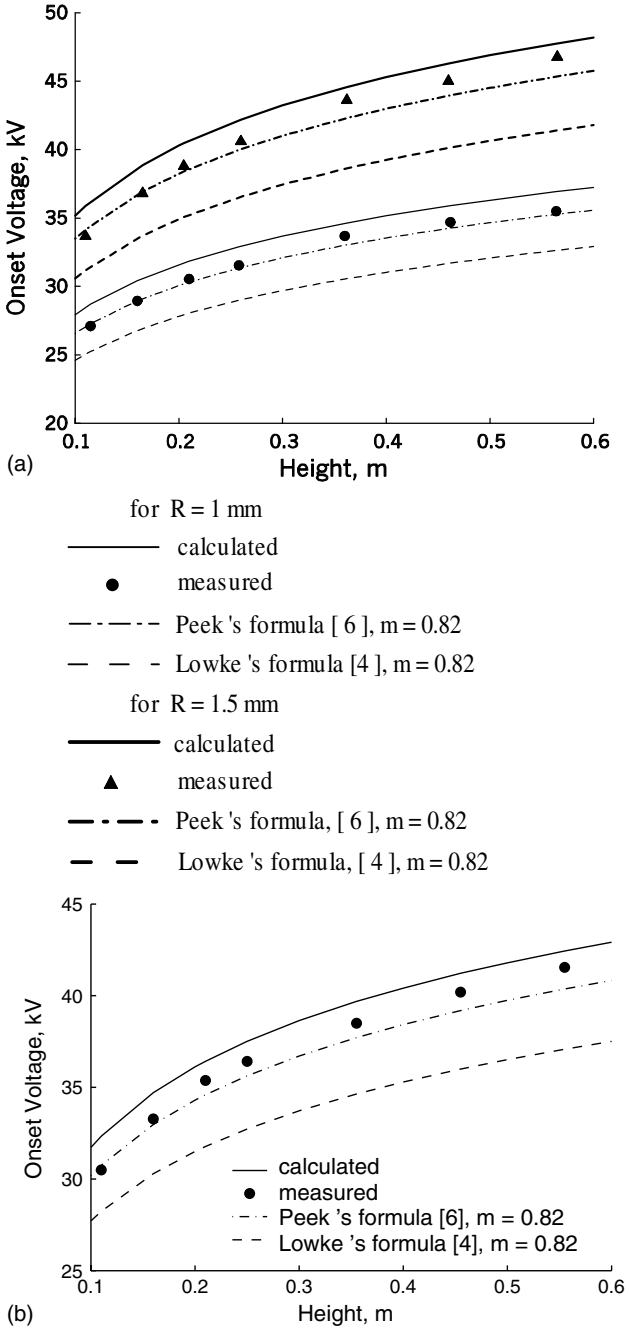

Figure 10. Measured and calculated onset voltage of corona for 7-strand conductors having radii 1 and 1.5 mm (*a*), and 1.25 mm (*b*).

of this research is that stranded conductor manufacturers try to develop stranded conductors with a large number of strands in the outer layer to enhance the corona onset voltage.

As shown in figure 10, most of the measured values lie over the onset values calculated by Peek's and Lowke's formulae; the calculated errors of the onset voltages (at the maximum value of irregularity factor, $m = 0.82$) are 3% and 13%, respectively. The calculated data seem to be in good agreement with experimental data in comparison with the data obtained from the empirical equations. The calculated onset voltage values agreed with those measured experimentally within 7%.

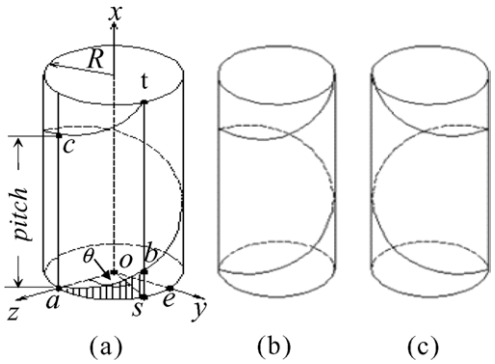

Figure A1. (*a*) A helix drawn along the circular conductor, (*b*) right-hand helix and (*c*) left-hand helix.

As the gap height or the conductor radius increases, the onset voltage increases. Unlike the empirical formulae, the present method has definite values of surface irregularity factor, m, and onset voltage of the corona.

8. Conclusions

1. Electric field distribution in stranded conductors-to-plane gaps is a three-dimensional field problem. The electric field is calculated using the charge simulation technique, where the stressed conductor is simulated by a number of helical charges.
2. To achieve good accuracy, it was found that the effective number of pitches depends on the gap height but it does not depend on the conductor radius and the type of stranding.
3. The accuracy of simulation is satisfied; the potential and the field deviation angle errors do not exceed 0.07% and 3.4° over the effective conductor surface, respectively.
4. The peak values of the surface electric field for stranded conductors divided by the peak value of a smooth cylindrical conductor having the same radius are nearly independent of the strand number n_o in the outer layer and equal approximately 1.4. This value agrees well with the values reported in the literature.
5. The larger the value of n_o, the smaller the region over which the electric field deviates from that of a smooth conductor in the vicinity of a conductor. Therefore, the onset voltage value increases and approaches that of a smooth cylindrical conductor as n_o increases.
6. The calculated onset voltage values agreed with those measured experimentally within 7%. In contrast, the data obtained from empirical equations are always smaller than the measured onset values.

Appendix A. Helix [10]

Let a point b (figure A1(a)) be in uniform motion along the generatrix st of a circular conductor and let the generatrix itself be in uniform rotation along the surface of the conductor. Then b describes a curve abc called a helix. The radius of the helix is the radius R of the conductor on which the helix is drawn.

If the motion of the point b is viewed from the base towards which it is moving, the rotation of the generatrix is either positive (counter-clockwise) or negative (clockwise).

The helix is termed right hand, (figure A1(b)), or left hand, (figure A1(c)), for the first case and the second case, respectively. The straight-line path ac (figure A1(a)) traversed by point b along the generatrix during one complete turn is called the pitch of the helix. The pitch of a right-hand helix is taken to be positive and that of a left-hand helix is taken to be negative. Right- and left-hand helixes (of one and the same radius and with the same absolute value of pitch) cannot be brought into coincidence. They are mirror symmetric since the segment sb is proportional to the arc $\overset{\frown}{as}$ as

$$sb : \overset{\frown}{as} = \text{pitch length}(L_\text{p}) : 2\pi R. \tag{A1}$$

Consider the x-axis as the axis of the conductor and the z-axis towards an arbitrarily chosen point a of the helix. Let $x = sb$ in figure A1(a) and the arc $\overset{\frown}{as}$ equals the conductor radius R times the rotation angle θ of the plane having an axial section oac to the new position ost. Then from equation (A1)

$$x = \frac{L_\text{p}}{2\pi}\theta. \tag{A2}$$

The projections of the helix on the x–y, x–z and y–z planes are sine, cosine and circle curves, respectively:

$$y = R\sin\left(\frac{2\pi x}{L_\text{p}}\right), \tag{A3}$$

$$z = R\cos\left(\frac{2\pi x}{L_\text{p}}\right). \tag{A4}$$

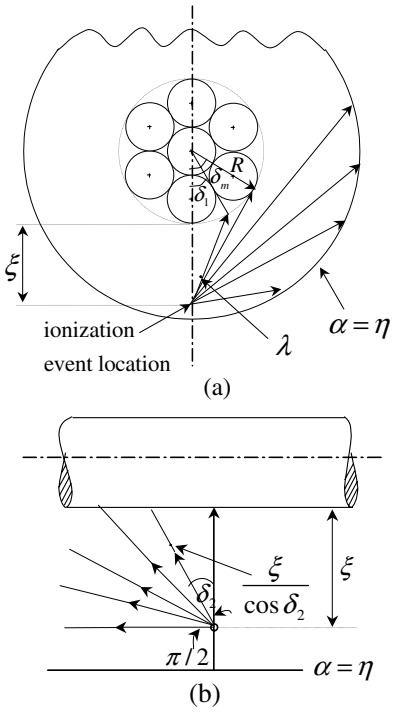

Figure B1. Diagram for the propagation of a photon in the ionization zone in the radial and axial directions from an ionization event along the route of the avalanche: (a) radial direction and (b) axial direction.

Appendix B. Calculation of geometry factor $g(\xi)$

For simplicity, during the calculation of the geometry factor $g(\xi)$ the stranded conductor is assumed to be a smooth conductor, figure B1. The geometry factor was given in [16] in terms of its radial and axial components $g_\text{rad}(\xi)$ and $g_\text{axial}(\xi)$ as $g(\xi) = g_\text{rad}(\xi)g_\text{axial}(\xi)$ and is expressed for wire-plane geometry as follows:

$$g_\text{axial}(\xi) = \frac{1}{\pi \mathrm{e}^{-\mu\xi}} \int_0^{\frac{\pi}{2}} \mathrm{e}^{-\frac{\mu\xi}{\cos\delta_2}}, \tag{B1}$$

$$g_\text{rad}(\xi) = \frac{1}{\pi \mathrm{e}^{-\mu\xi}} \int_0^{\delta_m} \mathrm{e}^{-\mu\sqrt{\lambda}}\,\mathrm{d}\delta_1, \tag{B2}$$

where

$$\delta_m = \cos^{-1}\left(\frac{R}{R+\xi}\right), \qquad \lambda = (R+\xi)^2 + R^2 + 2R(R+\xi)\cos\delta_1.$$

References

[1] Yamazaki K and Olsen R G 2004 Application of a corona onset criterion to calculation of corona onset voltage of stranded conductors *IEEE Trans. Dielectr. Electr. Insul.* **11** 674–80

[2] Nayak S K and Thomas M J 2005 An integro-differential equation technique for the computation of radiated EMI due to corona on HV power transmission lines *IEEE Trans. Power Delivery* **20** 488–93

[3] Arrillaga J 1998 *High Voltage Direct Current Transmission (IEE Power Engineering Series)* (London, UK)

[4] Lowke J J and Alessandro F D 2003 Onset corona fields and electrical breakdown criteria *J. Phys. D: Appl. Phys.* **36** 2673–82

[5] Abdel-Salam M and Shamloul D 1992 Computation of ion flow fields of AC coronating wires by charge simulation techniques *IEEE Trans. Electr. Insul.* **27** 352–61

[6] Peek F W 1929 *Dielectric Phenomena in High Voltage Engineering* (New York: Mc-Graw-Hill)

[7] Adams G E 1955 Voltage gradients on high voltage transmission lines *AIEE Trans.* **74** 5–11

[8] Lyer K S and Pillai K P P 1968 Analysis of irregularity factor of stranded conductor *Proc. IEE* **115** 364–7

[9] Whitehead J B 1911 The electric strength of air: II *AIEE Trans.* **28** 1857–87

[10] Vygodsky M 1971 *Mathematical Handbook—Higher Mathematics* (Moscow: Mir)

[11] El-Sewedy Industries, Egytech Cables, Cairo, Egypt

[12] Utmischi D 1979 Charge substitution method for three-dimensional high voltage fields *3rd Int. Symp. on High Voltage Engineering (Milan, 28–31 August 1979)* Paper 11.01

[13] Badawi Sayed Ahmed M 2007 Onset voltage of negative corona on stranded conductors *MSc Thesis* Faculty of Engineering, Banha University

[14] El-Bahy M M and Abou El-Ata M A 2005 Onset voltage of negative corona on dielectric-coated electrodes *J. Phys. D: Appl. Phys.* **38** 3403–11

[15] Abdel-Salam M, Anis H, El-Morshedy A and Radwan R 2000 *High Voltage Engineering-Theory and Practice* 2nd edn (New York: Dekker) pp 149–84

[16] Abdel-Salam M and Wiitanen D 1993 Calculation of corona onset voltage for duct-type precipitators *IEEE Trans. Indust. Appl.* **29** 274–80

[17] Abdel-Salam M, Turky A and Hashem A 1998 The onset voltage of coronas on bare and coated conductors *J. Phys. D: Appl. Phys.* **31** 2550–6

[18] Malik N H 1989 A review of the charge simulation method and its applications *IEEE Trans. Electr. Insul.* **24** 3–14